PERGAMON

Journal of Structural Geology 21 (1999) 1477–1490

JOURNAL OF STRUCTURAL GEOLOGY

www.elsevier.nl/locate/jstrugeo

Discontinuous grain growth in recrystallised vein quartz — implications for grain boundary structure, grain boundary mobility, crystallographic preferred orientation, and stress history

Bernhard Stöckhert*, Johannes Duyster

Institut für Geologie, Ruhr-Universität, D-44780 Bochum, Germany

Received 12 February 1998; accepted 13 March 1999

Abstract

Grain growth is a process driven by the reduction of interfacial free energy, leading to an increase in grain size and a reduction of the number of grains in a given volume of a single phase polycrystalline material. Discontinuous grain growth (DCGG), as opposed to normal grain growth (NGG) involves just a few grains (blasts) growing at the expense of a matrix, that itself undergoes much slower modification in grain size, hence producing a bimodal grain size distribution as a transient state prior to impingement of the blasts. Such a transient state has been found in a quartz layer in metamorphic rocks of the Sesia Zone, Western Alps. There, large strain-free quartz grains occur that reveal concave outward grain boundaries against a matrix of small grains with a pronounced crystallographic and a weak dimensional preferred orientation. The misorientation of the blasts with respect to the matrix grains systematically exceeds 30°. This finding suggests that the mobility of high-angle grain boundaries in a natural quartzite depends on the degree of their misorientation (among other factors), as known for metals and alloys. The width of the grain boundaries must be sufficiently small to allow for this effect. DCGG is promoted by a pronounced crystallographic preferred orientation (CPO), that leaves only a few grain boundaries with sufficient misorientation to be mobile. In contrast to NGG, DCGG wipes out any pre-existing CPO and information on activated glide systems or kinematics during the preceding stage of flow is lost after DCGG has gone to completion. A complementary new CPO could even develop, that could be difficult to interpret. With respect to tectonic history, interfacial free energy driven grain growth reflects a period of low stress annealing and thus constitutes a first order signal.

1. Introduction

Interfacial free energy (or tension) in a single phase crystalline solid is defined as

$$\gamma = (\mathrm{d}G/\mathrm{d}A)_{P,T,i} \quad (1)$$

with G denoting the free energy of the system, A the total area of grain boundaries. Pressure (P), temperature (T) and number of moles (i) are kept constant. In crystalline solids, interfacial free energies are on the order of 0.1–1 J m^{-2}. Minimisation of the free energy of any system involves increasing the grain size and the formation of appropriate low energy grain shapes. Notwithstanding its small contribution to the total free energy budget, interfacial free energy controls the microstructures, and hence some important physical properties of crystalline solids over a broad range of boundary conditions. Development of a low interfacial free energy microstructure requires grain boundary migration. This is a thermally activated process that generally proceeds at homologous temperatures (T/T_m, with T_m denoting the melting temperature in Kelvin) in excess of about 0.5. In general, the mobility of grain

* Corresponding author.
E-mail address: bernhard.stoeckhert@ruhr-uni-bochum.de (B. Stöckhert)

0191-8141/99/$ - see front matter
PII: S0191-8141(99)00084-X

boundaries increases with increasing misorientation between the grains. The dependence of the activation energy Q_{GBM} for grain boundary migration on misorientation behaves inversely to that of the grain boundary energy γ, as has been demonstrated by Fridman et al. (1975) for pure aluminium. The activation energy increases with decreasing misorientation, rendering low-angle grain boundaries less mobile. In absolute terms the mobility also depends on impurity content and other factors not considered here.

An increase in grain size, and respectively a reduction of the number of individual crystallites in a given volume of material, driven by a reduction in interfacial free energy, is referred to as grain growth. For the sake of clarity, the term grain growth should be avoided for processes where grain boundary migration is driven by other forces. If, for example, intergranular contrasts in stored strain energy are the driving force, the term recrystallisation should be used. On the other hand, the terms secondary or static recrystallisation, sometimes used synonymously with grain growth, are misleading. A microstructure with minimum interfacial free energy shows the following two features: (1) the interfaces between crystals are planar to minimise interfacial free energy, and (2) mechanical equilibrium is established at the grain edges (sometimes referred to as 'triple junctions' in two-dimensional cross-section). At mechanical equilibrium grain boundaries meet at angles specified by the following equation (Cotterill and Mould, 1976)

$$\gamma_1/\sin\theta_1 = \gamma_2/\sin\theta_2 = \gamma_3/\sin\theta_3 \quad (2)$$

with $\gamma_{1,2,3}$ denoting the grain boundary energies and $\theta_{1,2,3}$ the dihedral angles measured opposite to the boundaries with the identical label. For single phase crystalline solids, where interfacial free energies are uniform and, as a first approximation, independent of crystallographic orientation, mechanical equilibrium implies 120° angles between three interfaces meeting at a grain edge. Space filling (Underwood, 1970) does not allow for simultaneous fulfilment of both above postulates. Hence, a compromise between establishment of mechanical equilibrium angles at the grain edges and plane interfaces is required. This compromise grain shape is represented by the so-called β-tetracaidecahedron (Williams, 1968), with near-120° angles and simply curved interfaces. Because such microstructures obey the same topological principles as bubbles in a foam, they are referred to as foam structures (Underwood, 1970).

Geometrical constraints require that large grains with more than six sides in two-dimensional section display concave boundaries, whereas small grains have convex boundaries. If grain boundary migration is driven exclusively by interfacial free energy, curved

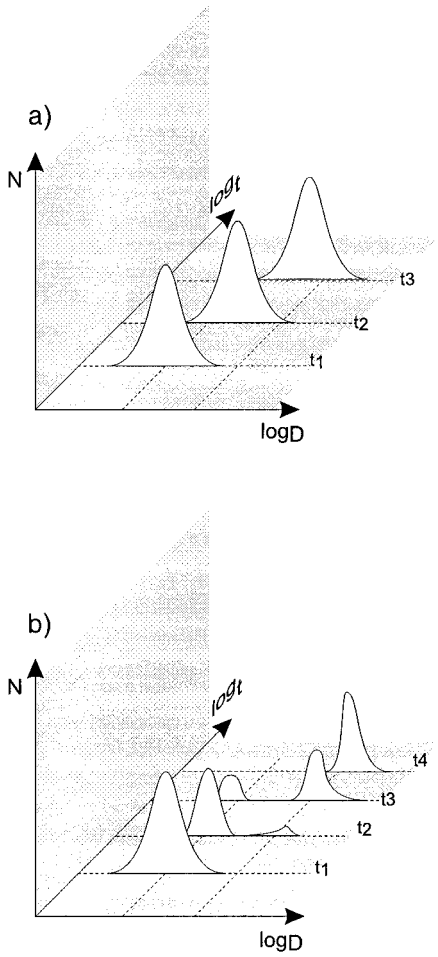

Fig. 1. Scheme visualising the grain size distribution as a function of time for (a) continuous grain growth, and (b) discontinuous grain growth.

boundaries always move towards their centres of curvature (e.g. Burke and Turnbull, 1952; Smith, 1964; Kingery et al., 1976) due to the higher free energy associated with an atom beneath a convex interface, as compared to one beneath a concave one. These relations cause small grains to shrink and large grains to grow. The self-organising nature of the grain boundary migration pattern thus results in a net increase in average grain size, i.e. grain growth. The driving force F for interfacial free energy driven grain boundary migration is

$$F = 2\gamma/(r_1 + r_2) \quad (3)$$

where r_1 and r_2 denote the principal radii of curvature and γ the grain boundary energy per unit area of the boundary (Stüwe, 1978). Thus, the driving force decreases with increasing radius of curvature. Consequently, grain growth eventually ceases when the grain size becomes large.

The topology of grain growth has been extensively discussed for metals and alloys (e.g. Feltham, 1956;

Cotterill and Mould, 1976). There, distinction is made between normal grain growth (NGG) and discontinuous grain growth (DCGG), depending on the transient grain size distribution during the course of the process (Cotterill and Mould, 1976; Detert, 1978). In NGG the grain size distribution remains log-normal throughout the process, whereas in DCGG it becomes bimodal, until the growing grains impinge (Fig. 1). This selective growth of individual grains in a matrix which does not undergo a significant modification of grain size, has also been termed exaggerated or anomalous grain growth (Cotterill and Mould, 1976, and references therein). We prefer the more specific term discontinuous grain growth (e.g. Detert, 1978).

In natural rocks, establishment of an interfacial free energy-controlled foam structure is taken as an indication of grain growth (Voll, 1960). Such microstructures have been widely reported (e.g. Voll, 1960; Spry, 1969; Vernon, 1976) for minerals where the grain boundary energy is nearly independent of the orientation of the interface with respect to the lattices of the adjacent grains. Under a wide range of conditions this holds for quartz, calcite, and olivine. Experimental work (e.g. Green et al., 1970; Tullis and Yund, 1982; Karato, 1989) has shown that grain growth in monomineralic aggregates of these rock-forming minerals principally obeys the rules established for metals. As in metals, grain growth is normally restricted to monomineralic aggregates and inhibited by dispersed second phase particles. Olgaard and Evans (1988) have studied this effect in experiments on calcite.

In minerals, for which the dependence of grain boundary energy on orientation is significant, unilaterally rational (e.g. Spry, 1969) grain boundaries predominate and a mosaic of hypidiomorphic grains develops instead of a foam structure. Since these interfaces are not curved, interfacial tension provides no effective driving force. Accordingly, experimental studies have shown that mineral aggregates with predominantly rational grain boundaries, e.g. anhydrite (Dell'Angelo and Olgaard, 1995) or coesite (Renner et al., 1997) do not undergo significant grain growth. However, since the dependence of grain boundary energy on orientation appears to vanish with increasing temperature, grain growth in these minerals can eventually become feasible at very high temperatures (Renner et al., 1997).

In contrast to normal grain growth (NGG), unequivocal evidence for discontinuous grain growth (DCGG) has not been reported so far for natural rocks, nor has this process been observed in experiments on rock-forming minerals. Here we present a conspicuous microfabric from a natural sample, which is interpreted to represent a frozen transient state developed during discontinuous grain growth of quartz.

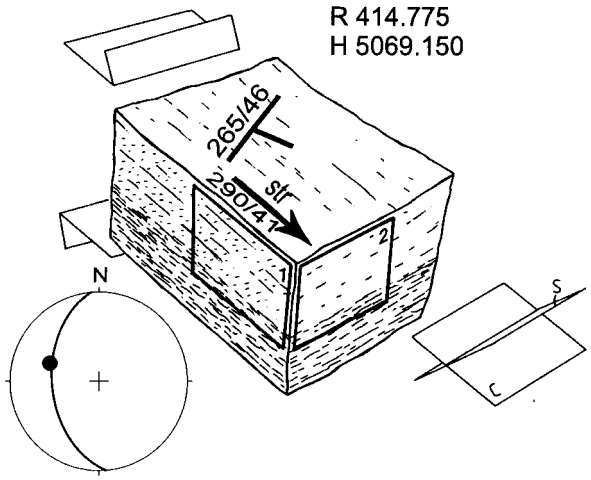

Fig. 2. Sketch of the sample. The orientation of foliation and stretching lineation, the oblique grain shape preferred orientation (shear sense indicator), and the positions of the examined thin sections are indicated.

2. Geologic setting

The specimen originates from the uppermost tectonic unit of the Sesia Zone (Western Alps, Italy), the so-called Seconda Zona Diorito Kinzigitica (Carraro et al., 1970; Dal Piaz et al., 1971; Avigad, 1996). Extensive volumes of pre-Alpine high-grade metamorphic basement with preserved microstructures and localised static retrogression are embedded in Alpine shear zones whose microstructure and mineral assemblages have been completely transformed. The metamorphic conditions at Alpine deformation have been estimated as $P = 10 \pm 3$ kbar, $T = 400 \pm 50$°C (Stöckhert, 1989; Avigad, 1996). The sample has been taken from banded blastomylonites exposed over several tens of metres in the upper Val Vogna, near Alpe Pioda di Sopra (R: 414.775; H: 5069.150) which formed during intense Alpine deformation of pre-Alpine high-grade metamorphic gneisses and pegmatites. The sample displays a compositional layering on the mm to cm scale. The almost pure quartz layers, a few millimetres thick and with a very high aspect ratio, presumably represent flattened quartz veins. They alternate with layers rich in white mica, chlorite, albite, epidote and garnet. Compositional layering and foliation dip with an angle of about 45° towards the west, the stretching lineation plunges at about 40° towards WNW. Microstructural shear sense indicators show a top to the WNW sense of shear (Fig. 2).

3. Analytical methods

For microfabric analysis of the quartz layer, the sample was cut normal to the compositional layering,

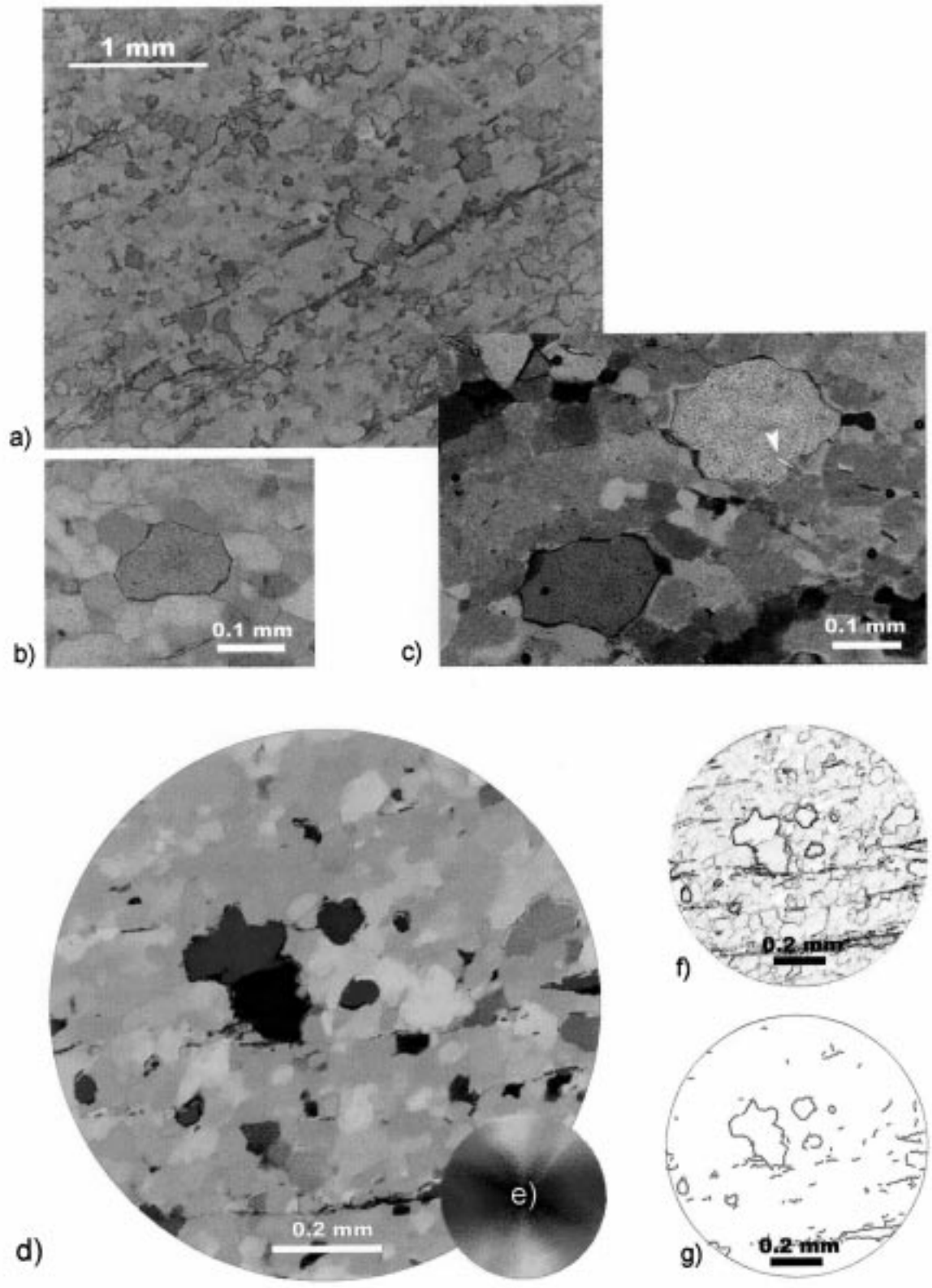

Fig. 3. (a) Microstructure of quartz layer. The pronounced crystallographic preferred orientation of the small M-grains and the distinct misorientation of many large B-grains is very evident. An oblique foliation is defined by the SPO of M-grains. Crossed polarisers; compensator red I 551 nm inserted, with n_γ parallel to the mylonitic foliation defined by mica (001) orientation. (b) and (c) B-grain in matrix of M-grains. Note the concave grain boundaries of the B-grain and the dihedral angles $\theta_{MM} > 120^\circ$. White arrow in (c) points to mica flake overgrown by the blast. Crossed polarisers; compensator red I 551 nm inserted. (d) AAVA orientation maps of B- and M-grains (see text for discussion and Appendix A for the method). (e) Colour coding scheme for map (d). (Equal area projection.) (f) Map of misorientations displayed as grey-values, dark colours indicate large misorientation angles, light colours indicate low misorientation angles. (g) High angle grain boundaries ($> 30^\circ$) extracted from map (e). Diameters of d, f, and g: 1 mm.

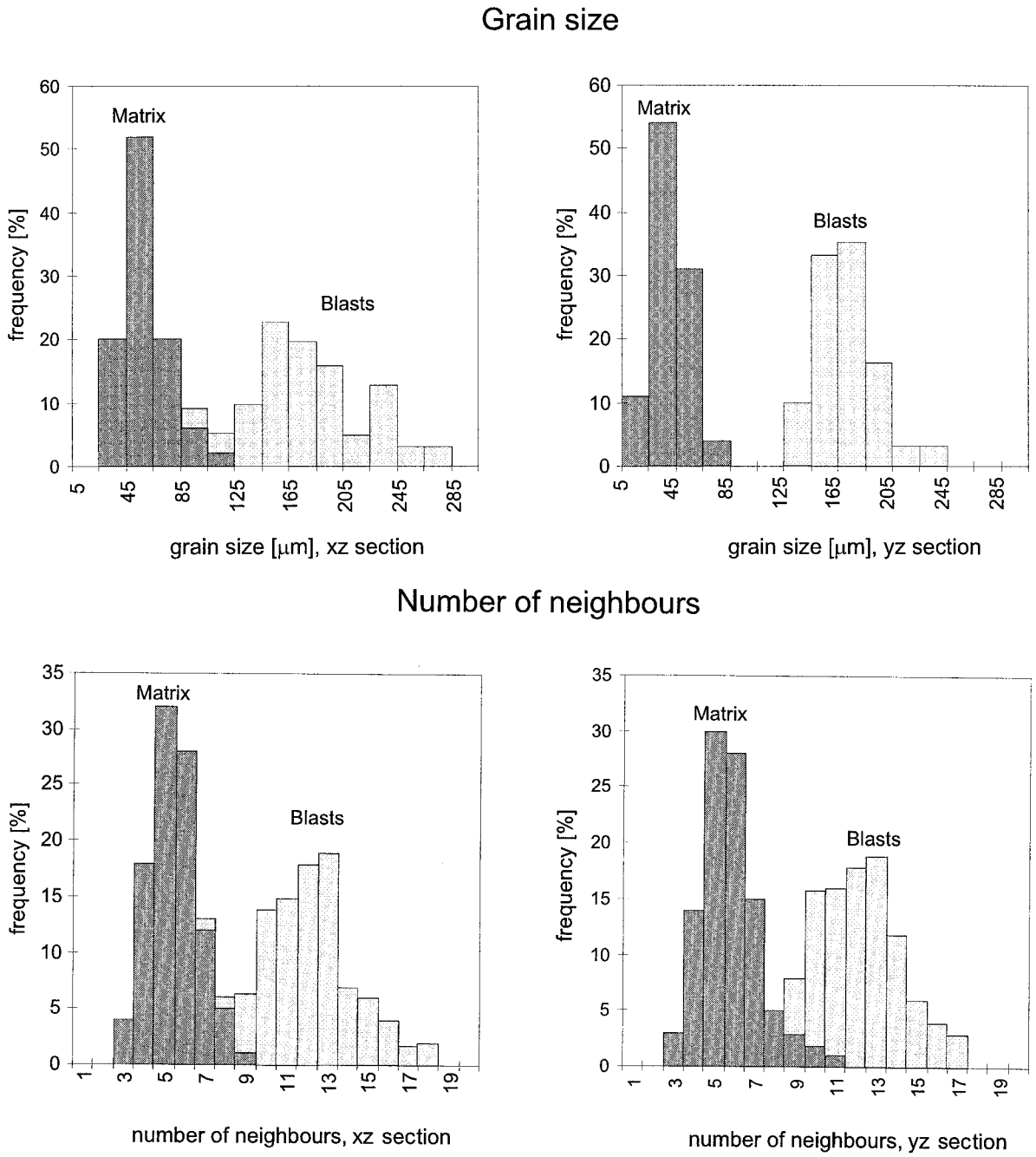

Fig. 4. Grain size (given as the diameter of a circle with equal area) and number of nearest neighbours in two-dimensional section. Left: Section parallel to lineation and normal to mylonitic foliation. Right: Section normal to lineation and mylonitic foliation.

both normal and parallel to the stretching lineation. Standard petrographic thin sections were prepared for image analysis and universal stage methods, polished sections for electron back scatter diffraction pattern (EBSD) analysis. The correlated microstructural and crystallographic orientation analysis was performed with five different methods:

1. The quartz *c*-axis orientation patterns were determined with a universal stage on a Zeiss Universal polarising microscope.
2. Grain size was measured interactively with an image analysis system. Grain size is displayed as the diameter of a circle with equal area.
3. The number of nearest neighbours in two-dimensional section was determined for a representative number of grains simply by counting.
4. The complete crystallographic orientations and thus the misorientations between individual grains were determined by EBSD (e.g. Lloyd and Freeman,

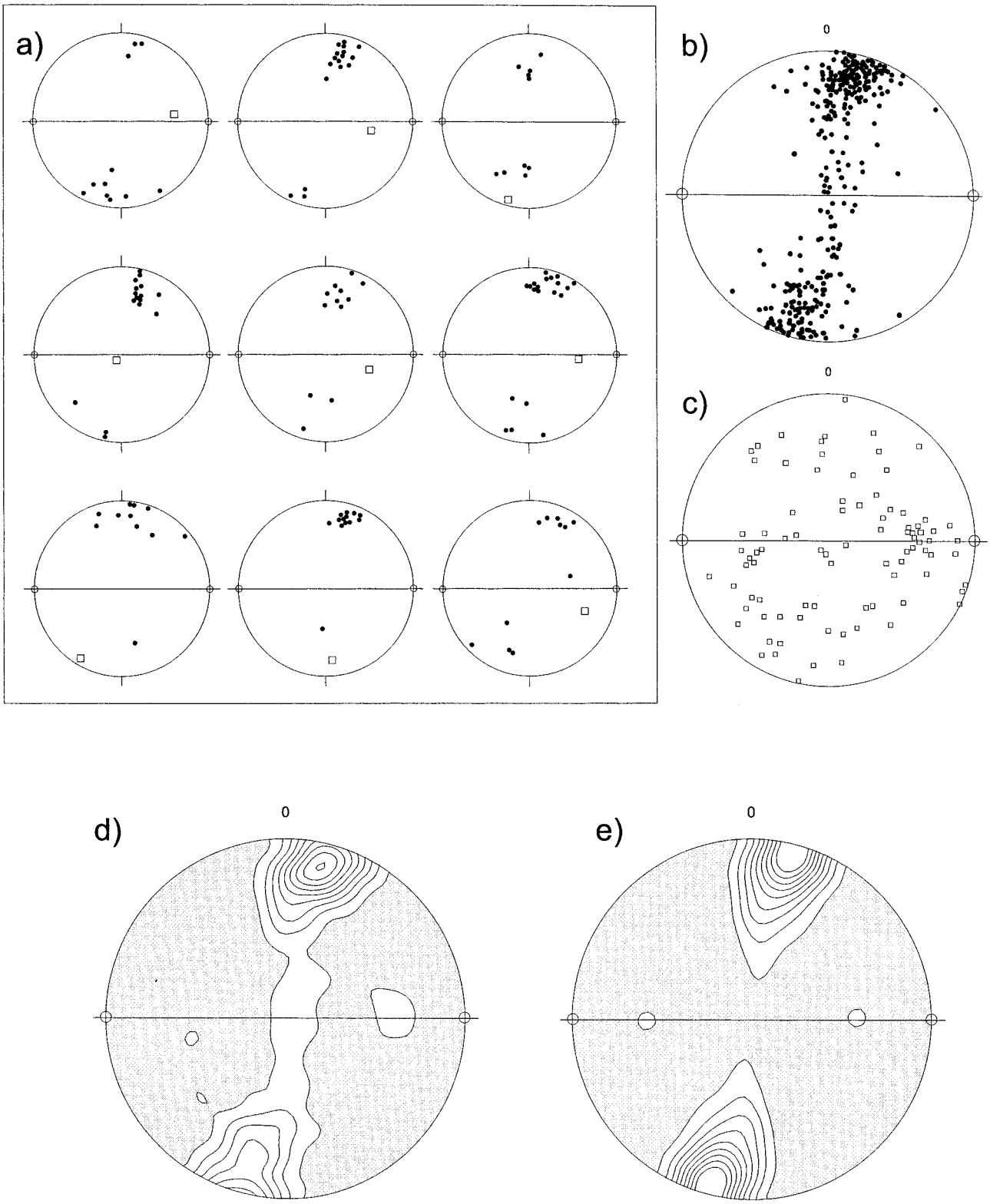

Fig. 5. (a) Orientation (*c*-axis) of B-grains and surrounding M-grains, determined with the universal stage. The number of surrounding M-grains reflects the relative size of the B-grains. Open squares: B-grain *c*-axes, filled circles: M-grain *c*-axes. (b) *c*-Axis orientation of M-grains, measured with the universal stage. (c) *c*-Axis orientation of B-grains, measured with the universal stage. (d) Bulk CPO (*c*-axis) derived by U-stage. (e) Bulk CPO (*c*-axis) derived by AAVA. All diagrams display the trace of the foliation and the orientation of the stretching lineation (open circles), equal area projection. See text and Appendix A for a description of methods.

1991). The patterns were recorded using a camera and detector assembly manufactured by *H. Jelen* and mounted on the *Jeol-850* SEM at Aarhus University, Denmark. Complete crystal orientations were computed by fitting the recorded Kikuchi bands using the *Channel+* software by *HKL-Software*, Hobro, Denmark. The automatic band detection mode of this software was not used. Instead, the position and width of the bands were marked manually. Since Kikuchi patterns for quartz are similar for Dauphiné twin positions (Olesen and Schmidt, 1990), all resulting orientations were checked for errors due to pseudo-symmetry effects. The *Channel+* software allows the interactive comparison between the simulated Kikuchi bands for both solutions and the recorded bands, allowing the minimisation of potential pseudo-symmetry effects.

5. To visualise and quantify the overall correlation between position, grain size and grain shape, and crystallographic orientation, we have computed AVA diagrams (AVA = Achsenverteilungsanalyse; Sander, 1950) using the software StereoNett (Duyster, 1996). This software applies image analysis techniques to calculate the azimuth and inclination of the quartz *c*-axes for every position within the field of view by recording the changing birefringence colours while the microscope stage is rotated by 90°, similar to the CIP method introduced by Panozzo Heilbronner and Pauli (1993). In the following, the method is referred to as AAVA (Automatized AchsenVerteilungs Analyse) and a more detailed description of the procedure is given in the Appendix A.

All these methods are to a large extent complementary and the results are internally consistent.

4. Quartz microstructures and crystallographic orientation

4.1. Microstructure

In the pure quartz layers of the blastomylonite, the microstructure suggests that the original vein quartz has been completely recrystallised during progressive deformation by dislocation creep, with no relics of earlier fabrics preserved. The quartz grain-size distribution is markedly bimodal, with $>90\%$ of the volume made up by a matrix with a grain size of about 0.04 mm (M-grains for matrix-grains), and $<10\%$ by isolated large grains with a grain size of 0.2–0.4 mm (B-grains for blasts, see Figs. 3 and 4).

In sections parallel to the stretching lineation, the anisometric shape of the M-grains in pure quartz layers defines an oblique foliation (Means, 1981; Lister and Snoke, 1984; see Fig. 3), whereas isolated white mica flakes (mica fish) are aligned with (001) parallel to the pronounced mesoscopic compositional banding. The oblique foliation defined by the shape preferred orientation (SPO) of the long axes of the M-grains makes up an angle of roughly 45° with the compositional layering. The asymmetry of this oblique foliation indicates a top to the WNW sense of shear and is fully consistent with the shape of the mica fish (e.g. Simpson and Schmid, 1983) and asymmetric strain shadows at garnets in adjacent polymineralic layers. During flow by dislocation creep, development of the oblique foliation by progressive flattening and rotation of the grains was continuously counteracted by recrystallisation. This resulted in a steady state foliation as described by Means (1981). The microstructure of the M-grains is interpreted to represent a synkinematic state, only slightly modified after deformation had ceased.

The shape of the B-grains tends to be anisometric as well, with their long axis oriented parallel to the oblique foliation, but their axial ratio is smaller when compared to the M-grains. The spatial distribution of B-grains is random. Depending on the volume of the individual B-grains, they are surrounded by up to 20 M-grains as nearest neighbours in two-dimensional section (Figs. 3 and 4).

Both type M and B grains show no evidence for significant concentrations of distributed geometrically necessary dislocations (undulatory extinction). The grains can be characterised as 'optically strain-free'. As seen in the TEM, dislocation densities are below about 10^{11} m^{-2} with no discernible contrast between M- and B-grains.

The grain boundary pattern is simple. The boundaries tend to be straight or simply curved. Dihedral angles measured within B-grains in contact with two M-grains systematically exceed 120°, whereas angles close to 120° prevail at edges between three M-grains.

4.2. Quartz crystallographic preferred orientation

The presence of a pronounced crystallographic preferred orientation of the M-grains is readily visualised by insertion of the gypsum plate (compensator red I, 551 nm, as shown in Fig. 3a). The orientation of the *c*-axes of a representative number of grains was measured using a universal stage, with M- and B-grains being measured separately (Fig. 5a–c). The B-grains were identified by means of their size (>0.2 mm). In measuring the M-grains (grain size up to 0.04 mm, see Fig. 4), only grains with grain boundaries steeply inclined with respect to the section plane were considered. Small grains with gently dipping boundaries were omitted since they may constitute truncated B-grains.

The *c*-axis preferred orientation of M-grains is represented by a slightly asymmetric girdle around the stretching lineation (Fig. 5b). The preferred *c*-axis orientation normal to the stretching lineation indicates that ⟨*a*⟩ slip operated during deformation. The majority of the *c*-axes are oriented at a high angle to the foliation. This pattern suggests that slip took place predominantly on the basal plane (0001). Additional ⟨*a*⟩ glide on rhomb and prism planes is indicated by the continuity of the girdle. These glide systems are considered to be operative at moderate temperatures (Hobbs, 1985), fully consistent with the maximum temperatures of $400 \pm 50^{\circ}C$ suggested for the Alpine overprint (Stöckhert, 1989). The slight asymmetry of the girdle corresponds to the top to the WNW sense of shear inferred from the microstructures (e.g. Bouchez et al., 1983; Price, 1985; Law, 1990).

In contrast to the M-grains, the B-grains display no marked *c*-axis preferred orientation. However, in the equal area projections the areas close to the *Z* direction (normal to the foliation) appear to be unpopulated, in marked contrast to the maximum population density of these areas found for the M-grains (Fig. 5c).

In addition to the U-stage analysis, AAVA has been applied. The sample constitutes an ideal site for this method. Fig. 3(d) shows an AAVA map and the corresponding colour coding scheme (Fig. 3e). From the AAVA maps (minimum-)misorientation maps were computed (Fig. 3f). *c*-Axis azimuth and dip are computed at every pixel position in the AAVA map. The misorientation map displays the angular difference of the *c*-axes measurements between neighbouring pixels. Within one grain this difference remains within the limits of error of the measurement, whereas at grain boundaries this contrast is larger. Since the azimuth of the *c*-axes is available only without polarity, the angle between the axes cannot be computed without ambiguity. Two solutions can be found, one of which is wrong. As a convention, the smaller of the two angles is displayed in the misorientation map. Additionally, grain boundaries with a misfit of more than 30° were extracted from the misorientation map and displayed in Fig. 3(g). Note, that some of the horizontal boundaries in the misorientation maps are artefacts related to phase boundaries between quartz and mica. A bulk *c*-axis distribution pattern computed from the AAVA data (Fig. 5e) is remarkably consistent with those obtained by U-stage analysis (Fig. 5d).

4.3. Orientation of blasts relative to the adjacent matrix grains

The *c*-axis orientations for individual B-grains and all adjacent M-grains (in two-dimensional section), determined with the universal stage, are displayed in Fig. 5(a). The diagrams reveal that the *c*-axis orien-

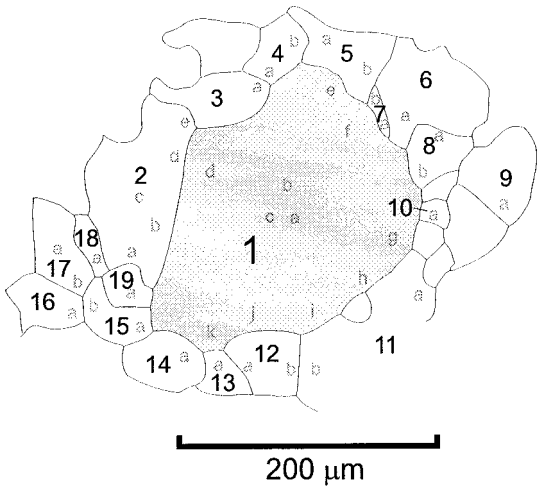

Fig. 6. Grain boundary tracing of a B-grain in a matrix of M-grains (domain 1).

Table 1
Domain 1

Measuring positions		Rotation axis		Rot. angle
Matrix–blast relations				
1d	2b	92	34	97
1d	2c	132	13	84
1d	2d	131	14	85
1d	2e	134	13	88
1d	3a	332	17	−73
1e	5a	351	25	−82
1f	7b	354	24	−79
1g	8a	328	4	−84
1g	10a	301	14	−76
1h	11a	309	12	−67
1i	11b	311	16	−62
1j	12a	70	61	−72
1j	12b	68	61	−72
1k	2b	91	34	−97
1k	13a	95	42	−93
1k	15a	338	18	−80
1k	19a	338	17	−80
2e	5b	350	25	−81
3e	7a	351	25	−79
Matrix–matrix relations				
3a	4a	49	62	−59
4b	5a	68	68	−24
8a	7b	133	66	−42
8a	9a	0	66	−34
12b	11b	31	2	−85
13a	12a	263	5	39
14a	13a	225	82	60
14a	15a	39	69	52
15a	19a	249	62	−1
16a	17a	172	21	60
17a	18a	1	25	26
18a	2b	6	23	12
19a	2b	4	10	26

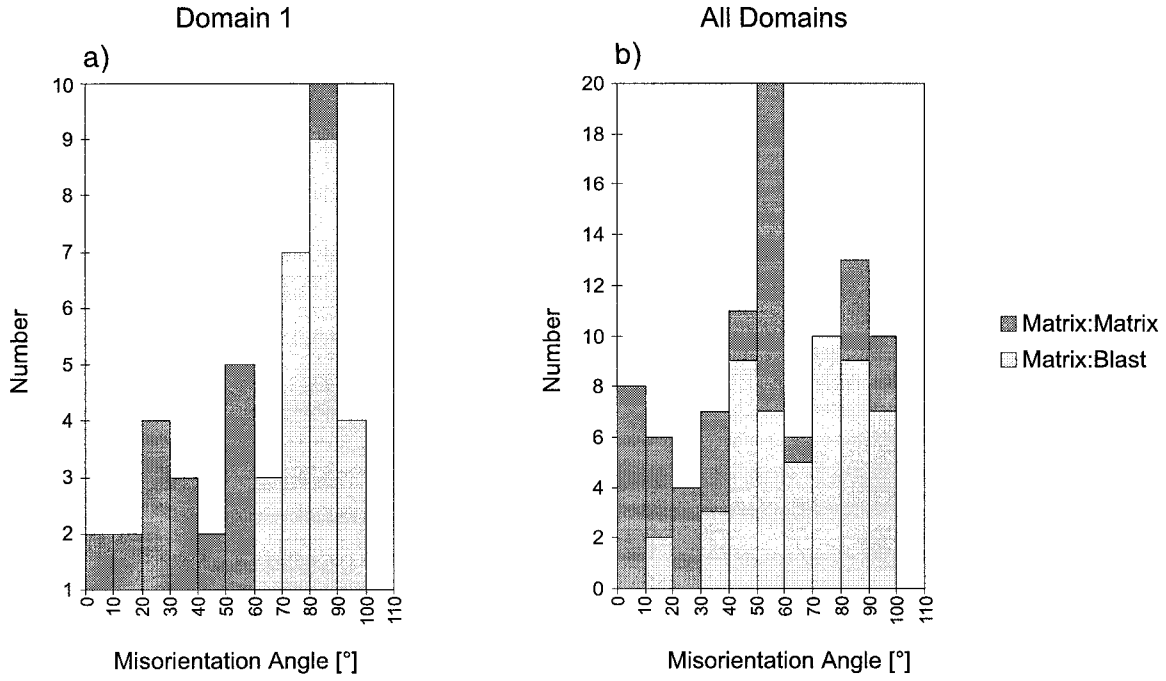

Fig. 7. Frequency of misorientation angles between adjacent grains, (a) for domain 1 (cf. Fig. 6) and (b) for all domains analysed with EBSD.

tation of the B-grain deviates from the matrix preferred orientation cluster by at least 30°. Since the full crystallographic orientation of quartz cannot be determined by optical methods, the orientation relations between B-grain and surrounding M-grains has been additionally determined by EBSP for 101 grains in five domains. All domains contain one B-grain surrounded by M-grains. The results are displayed in Figs. 6 and 7 and Table 1.

Fig. 6 shows an example of grain boundary tracings in an area for which the orientations of the individual grains were determined using EBSD. Table 1 displays the misorientation between each individual M-grain and the central B-grain in terms of rotation angle and rotation axis as well as the misorientation between the adjacent M-grains. Due to the crystal symmetry of quartz, six solutions exist for every grain boundary. Only the solution with the smallest rotation angle is given. Grain boundaries between two M-grains reveal misorientations between 5 and 30°, whereas grain boundaries between B- and M-grains systematically show larger misorientations. This is also shown by the histogram plot displaying the frequencies of the misorientation angles (Fig. 7a, b).

5. Discussion

The microstructure of the quartz layer and the crystallographic preferred orientation of the M-grains reflect intense non-coaxial deformation by dislocation creep with complete dynamic recrystallisation. The optically strain-free grains and the plane or simply curved grain boundaries show that stress relaxation subsequent to that stage of flow occurred at elevated temperatures. These temperatures were high enough to allow for postkinematic recrystallisation and recovery, and finally for grain boundary migration driven by interfacial free energy, i.e. grain growth. The preservation of the oblique shape preferred orientation, representing a steady state foliation as described by Means (1981), suggests that the synkinematic recrystallised grain size of the M-grains has not been modified significantly by grain growth. As such, the grain size of the M-grains still allows a rough estimate of flow stress. For the given M-grain size on the order of 0.04 mm a flow stress of about 50 MPa is derived using the theoretical calibration proposed by Twiss (1977).

The large B-grains are strain-free and do not contain any subgrains. In places they have overgrown white mica flakes oriented with their basal plane (001) parallel to the mylonitic foliation (Fig. 3c, see arrow). This shows that the B-grains do not represent relic grains in a core and mantle type microstructure, but that they have grown to their present size subsequent to the stage of flow. The bimodal grain size distribution developed during this stage of annealing is indicative of discontinuous grain growth (DCGG).

The phenomenology of DCGG has been studied in a variety of metals and alloys (Cotterill and Mould, 1976 and references therein; Detert, 1978; Cahn, 1983).

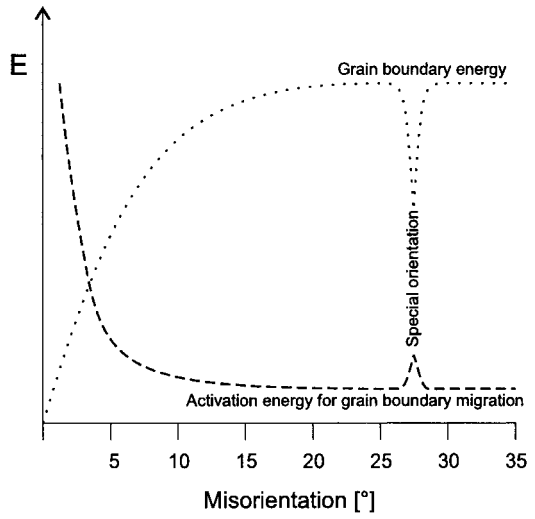

Fig. 8. Schematic diagram showing the general dependence of the interfacial free energy and of the activation energy for grain boundary migration on misorientation.

Cahn (1983) has summarised the characteristic features of DCGG as follows:

1. The large grains develop from pre-existing grains present in the initial microstructure.
2. The initial stage of DCGG is sluggish and comprises an incubation stage.
3. The grains to grow are generally larger than the average and their orientation differs from the overall crystallographic preferred orientation.
4. Normal grain growth (NGG) must be inhibited in order to allow for DCGG.
5. When DCGG has gone to completion, the resulting crystallographic preferred orientation differs from that present at the start of the process.
6. A well-defined minimum temperature must be exceeded for grain growth to proceed. The least number of growing grains is observed if this temperature is only slightly exceeded, whereas higher temperatures lead to larger numbers of growing grains and a smaller final grain size. Rapid heating to high temperatures induces NGG.

For the fabric development in our natural sample we have no information on time derivatives. The microfabrics of quartz, however, are fully consistent with the latter statements of Cahn (1983). Hence, the underlying process is considered as an example of what has been termed texture-induced abnormal grain growth (Beck and Sperry, 1949; Beck, 1954; Cotterill and Mould, 1976; Detert, 1978). In this case the material, at the onset of annealing, has a strong crystallographic preferred orientation acquired during a preceding stage of deformation by dislocation creep with concomitant dynamic recrystallisation. The pronounced crystallographic preferred orientation gives rise to a high proportion of grain boundaries with low misorientation. These have a low interfacial free energy associated with a low mobility (Cotterill and Mould, 1976), that inhibits the progress of NGG (Fig. 8). Only a few grains with an incidentally larger misorientation with respect to their neighbours are surrounded by higher angle grain boundaries, that are more mobile (Cotterill and Mould, 1976; Detert, 1978). In order to grow, driven by a reduction of interfacial free energy, these grains must also have a diameter that is larger than that of the surrounding grains. Only then is the shape of the grain boundaries concave allowing for their outward migration. This incipient stage of DCGG is the least understood in metals (Cahn, 1983) and deserves some more discussion.In principle, there appear to be two possible scenarios of microstructural evolution in the transitional stage between waning deformation and onset of low stress annealing, both of which could create a microstructure allowing for subsequent DCGG.

(a) The B-grains had already started to grow in the final stage of recrystallisation, growing selectively due to their higher grain boundary mobility. This would imply a lower dislocation density of grains in

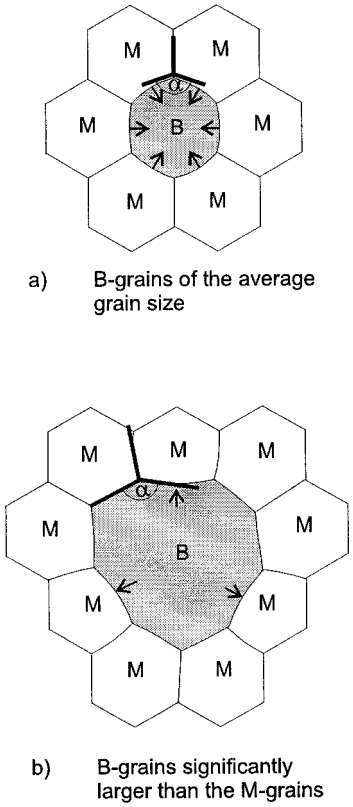

Fig. 9. Dihedral angles at grain edges between two grains in 'M-' and one grain in 'B-orientation'. (a) Grains in 'B-orientation' with average grain size develop convex grain boundaries. These grains will shrink during grain growth (arrows). (b) Grains significantly larger than the surrounding M-grains develop concave grain boundaries. These grains will grow during grain growth (arrows).

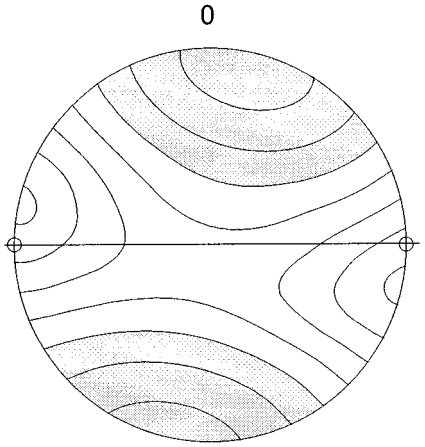

Fig. 10. Hypothetical complementary texture, that would have developed if DCGG had gone to completion and B-grains impinged on each other. Density in grey area is less than average.

orientations that do not favour glide, as compared to the surrounding M-grains in an easy glide orientation. The grains in B-orientation would otherwise have been eliminated during that stage of primary recrystallisation.

(b) The B-grains are initially a selection of grains which incidentally have an above average grain size. Originally, after cessation of flow, there would be more grains with an orientation differing from that of the present matrix-texture. However, those with diameters below average would shrink and disappear during grain growth.

Scenario (b) appears to be less probable due to the following consideration. In mechanical equilibrium, according to Eq. (3), dihedral angles in the grains of B-type orientation at M–M–B grain edges should exceed 120° because of the low grain boundary energy of the M–M interface. Therefore, even six-sided (in two-dimensional section) grains in B-type orientation, with the same grain size as their neighbouring M-grains, will have convex grain boundaries. Due to this curvature, the grain boundaries will migrate inward driven by interfacial free energy and the grains will be consumed (Fig. 9a). B-grains will only grow if their diameter is significantly larger than the average matrix grain size at the onset of grain growth (Fig. 9b). Only then would the grain boundaries be concave and move outwards. Although an unequivocal record for the processes in the critical incubation stage of DCGG is lacking, the considerations given above suggest that the above-average grain size of later B-grains is acquired during the waning stage of primary recrystallisation and that dislocation densities in grains not favourably oriented for glide remain below those in grains in easy glide orientations.Selective growth of grains with a high degree of misorientation with respect to the matrix CPO results in the destruction of the latter. While the B-grains are growing, the original matrix orientations become progressively underrepresented. Finally, upon impingement of the B-grains, a weak new CPO complementary to the original texture is expected to be developed. In the present case, this new CPO would look like that displayed in Fig. 10 (complementary texture) as opposed to the synkinematically developed original CPO displayed in Fig. 5(d). As such, postkinematic texture-induced DCGG obliterates any information on activated glide systems and strain path, usually obtained by texture analysis (Price, 1985). In view of this effect of DCGG, the absence of a conspicuous crystallographic preferred orientation in coarse-grained quartz ribbons in blastomylonites must not be misinterpreted. It cannot be taken as an indication that deformation was by a mechanism other than dislocation creep, or that the quartz ribbon had formed by some process of mass transfer even after deformation. A missing or difficult to interpret weak CPO in highly strained rocks may be the result of DCGG.

Following argument (6) from the above list of observations in metals (Cahn, 1983), DCGG is expected to be favoured by moderate temperatures. As in the present example, this could mean temperatures between about 350 and 450°C for quartz. Higher temperatures, or rapid heating during contact metamorphism, would disfavour the required inhibition of NGG. The pronounced crystallographic preferred orientations in quartz, the prerequisite for texture induced DCGG, develop readily during deformation by dislocation creep at these moderate temperatures due to the limited number of activated glide systems (e.g. Hobbs, 1985).

Summing up, the sensibility of DCGG to temperature and stress history requires a specific tectonic scenario for the process to proceed. This tectonic scenario implies the following stages and boundary conditions:

1. Accumulation of sufficient strain by dislocation creep leads to development of a pronounced crystallographic preferred orientation.
2. Relaxation of differential stress takes place at moderate temperatures that just allow for recrystallisation and recovery. After contrasts in stored strain energy have been eliminated, DCGG can proceed if the microstructural prerequisites discussed above are fulfilled.
3. Rocks showing frozen microstructures indicative of DCGG must have resided for a considerable time at elevated temperatures and very low differential stress. They can have experienced neither renewed loading to higher differential stress, nor significant reheating, as both would lead to the destruction of the DCGG-microstructure.

Note, that this tectonic scenario is necessary but poss-

ibly not sufficient, as other factors like grain boundary impurities may impede DCGG.The example presented in this paper shows that the principles of DCGG established for metals (Cotterill and Mould, 1976; Cahn, 1983 and references therein) also hold for quartz in deformed rocks. This suggests that the dependence of grain boundary mobility on misorientation is similarly effective in a 'dirty' natural silicate system, as that observed in high purity metals and alloys (e.g. Haessner and Hofmann, 1978). The inferred strong dependence of mobility on misorientation is interpreted to rule out a high grain boundary width and the presence of a continuous grain boundary phase or a fluid film. For quartz, this has already been postulated by Voll (1961) based on the observation of systematic orientation relations between adjacent grains and crystallographically controlled preferred alignment of grain boundaries.

6. Conclusions

The microfabrics of quartz in the investigated sample are interpreted as a frozen transient state developed during texture induced discontinuous grain growth. This finding bears the following implications:

1. The mobility of grain boundaries in quartz depends on the misorientation of the neighbouring grains. Increasing misorientation means higher mobility, and hence lower activation energy for grain boundary migration, as also has been observed for metals and alloys.
2. The structure of grain boundaries in a natural quartzite allows for a marked influence of small differences in misorientation on grain boundary mobility. This suggests a narrow grain boundary width, notwithstanding all impurity effects expected for natural rocks.
3. A pronounced crystallographic preferred orientation produced by deformation in the dislocation creep regime is a prerequisite for texture induced discontinuous grain growth. During subsequent annealing, this process leads to selective growth of grains with significant deviation in orientation from the surrounding matrix. The pre-existing crystallographic preferred orientation becomes completely wiped out upon impingement of the blasts. Absent or weak and poorly understood patterns of crystallographic preferred orientation in quartz ribbons of blastomylonites are suspected to result from discontinuous grain growth.
4. Microstructures controlled by interfacial free energy indicate that, at the stage of grain growth, the magnitude of differential stress was too low to drive dislocation creep and that the temperature was high enough for this thermally activated process to proceed. Furthermore, preservation of these microstructures indicates that differential stress, as a function of temperature, must have remained sufficiently low to prevent destruction of the microstructure during subsequent cooling and exhumation. As such, the observation of microstructures indicative of grain growth can be taken as a first order signal for the reconstruction of tectonic histories.

Acknowledgements

We are indebted to Niels Østerby Olesen at Aarhus University, who kindly provided access to the EBSP facilities, for help and advice during the measurements. We thank Brian Evans and Marc Jessel for their detailed reviews. Stuart Thomson is thanked for improving the English.

Appendix A. Description of the AAVA procedure

AAVA is an image analysis technique to calculate azimuth and dip of the quartz *c*-axes using a polarising microscope, a video camera and a frame grabber. While the microscope stage is turned by 90° the changing birefringence colours at every position within the field of view are recorded. The maximum birefringence colours of quartz in a thin section of 30 μm thickness range between black and first order white and are a function of the dip angle of the *c*-axis. Extinction occurs when the *c*-axis is parallel to one of the crossed polarisers. This signal is repeated four times, by turning the stage by 360°. Using a gypsum compensator plate (551 nm, red I), two of the four quadrants show additive, and two subtractive colours. The software uses this information to calculate azimuth and dip of the *c*-axis.

The AAVA procedure is similar to the CIP method of Panozzo Heilbronner and Pauli (1993), but simpler. The main differences between CIP and AAVA are the following:

1. The azimuth determined by AAVA is bipolar (i.e. no distinction is made between a dip to the NE or the SW). The computed texture will always display at least a monoclinic symmetry. Since the *c*-axis distribution of the analysed sample actually shows monoclinic symmetry as checked by conventional *c*-axis analysis this is no disadvantage.
2. During image acquisition the polarisers are kept fixed, just the specimen is turned using the microscope stage. The single frames are rotated and fitted onto each other by the software. This makes the method easier and faster.

The hardware set-up required is 'very basic' and no

interactive post-processing is needed. Instead of a monochrome infrared camera and monochromatic light, we used a colour video camera and ordinary white light. The specimen is not tilted and no manual fitting of frames, smoothing or filtering is required. The procedure is outlined in the following.First, two colour images with crossed polarisers and gypsum plate inserted are recorded with an angle of 45° to each other. These images are coded as ternary (three-bit) images using a colour model that distinguishes between three cases:

(A) Yellow–orange birefringence colours indicate subtraction; n_γ of the compensator and the azimuth of n_γ of the quartz grain, which is the direction *c*-axis, are at an angle larger than 45°.

(B) Magenta colour or first order red (551 nm) occurs when the *c*-axis is parallel to one of the polarisers or normal to the section plane.

(C) Blue to cyan birefringence colours indicate addition. This occurs when the angle between n_γ of the compensator plate and the azimuth of the quartz *c*-axis is less than 45°.

After combining the two images, nine possible cases can be distinguished. Thus, from these two images, the azimuth of the *c*-axis at every point (pixel) is determined with an accuracy of about $180°/8 = 22.5°$. Magenta in both images indicates a steep orientation of the *c*-axis with respect to the section plane. After removing the compensator plate the thin section is turned around 90° and grey value images are captured at 5° intervals. Grey value (=luminance) images were chosen, because the spatial resolution of a standard (s-vhs) colour video camera is much better for the luminance than for the crominance signal. While turning the microscope stage, the software rotates the captured images back to 0°. The intensity of the luminance signal as a function of the rotation angle at every point in the image series approximately follows a $\sin^2$ curve. The phase shift of this signal is used to refine the azimuth information, the amplitude (=luminance at maximum birefringence colour) is used to determine the dip of the *c*-axis. The result is a map of *c*-axes orientations (spatially resolved texture) from which a density distribution diagram (bulk texture) can be computed. The map is stored as a three channel image in a format which displays *c*-axis azimuth, dip and quadrant coding in the different channels. The angular resolution of this method is about 2–5° for the bipolar azimuth information, that of the dip depends on the dip angle. Altogether, the resulting errors are comparable to those occurring during measurements with a universal stage.AvaGenerator and StereoNett and are programs for the MS-Windows operating system which can be downloaded at: http://homepage.ruhr-uni-bochum.de/Johannes.P.Duyster/stereo/stereo1.htm

References

Avigad, D., 1996. Pre-collisional ductile extension in the internal western Alps (Sesia zone, Italy). Earth and Planetary Science Letters 137, 175–188.

Beck, P.A., 1954. Annealing of cold worked metals. Advances in Physics 3, 245–324.

Beck, P.A., Sperry, P.R., 1949. Effect of recrystallization texture on grain growth. Transactions of the Metallurgical Society AIME 185, 240–248.

Bouchez, J.L., Lister, G.S., Nicolas, A., 1983. Fabric asymmetry and shear sense in movement zones. Geologische Rundschau 72, 401–419.

Burke, J.E., Turnbull, D., 1952. Recrystallization and grain growth. Progress in Metal Physics 3, 220–292.

Cahn, R.W., 1983. Secondary recrystallization. In: Cahn, R.W., Haasen, P. (Eds.), Physical Metallurgy. Elsevier, Amsterdam, pp. 1658–1671.

Carraro, F., Dal Piaz, G.V., Sacchi, R., 1970. Serie de Valpelline e II Zona Diorito–Kinzigitica sono i relitti di un ricomprimento proveniente dalla zona Ivrea–Verbano. Memorie della Società Geologica Italiana 9, 197–224.

Cotterill, P., Mould, P.R., 1976. Recrystallization and Grain Growth in Metals. Surrey University Press, London.

Dal Piaz, G.V., Gosso, G., Martinotti, G., 1971. La II Zona Dioritico–Kinzigitica tra la Val Sesia e la Valle d'Ayas (Alpi occidentali). Memorie della Società Geologica Italiana 10, 257–276.

Dell'Angelo, L.N., Olgaard, D.L., 1995. Experimental deformation of fine-grained anhydrite: Evidence for dislocation and diffusion creep. Journal of Geophysical Research 100, 15425–15440.

Detert, K., 1978. Secondary recrystallization. In: Haessner, F. (Ed.), Recrystallization of Metallic Materials. Riederer, Stuttgart, pp. 97–110.

Duyster, J., 1996. StereoNett 2.0, University of Bochum.

Feltham, P., 1956. Grain growth in metals. Acta Metallurgica 5, 97–105.

Fridman, E.M., Kopezky, C.V., Shvindlerman, L.S., 1975. Effects of orientation and concentration factors on migration of individual grain boundaries in aluminium. Zeitschrift für Metallkunde 66, 533–539.

Green, H.W., Griggs, D.T., Christie, J.M., 1970. Syntectonic and annealing recrystallization of fine-grained quartz aggregates. In: Paulitsch, P. (Ed.), Experimental and Natural Rock Deformation. Springer, Berlin, pp. 272–335.

Haessner, F., Hofmann, S., 1978. Migration of high angle grain boundaries. In: Haessner, F. (Ed.), Recrystallization of Metallic Materials. Riederer, Stuttgart, pp. 63–95.

Hobbs, B.E., 1985. The geological significance of microfabric analysis. In: Wenk, H.-R. (Ed.), Preferred Orientation in Deformed Metals and Rocks: An Introduction to Modern Texture Analysis. Academic Press, London, pp. 463–484.

Karato, S., 1989. Grain growth kinetics in olivine aggregates. Tectonophysics 168, 255–273.

Kingery, W.D., Bowen, H.K., Uhlmann, D.R., 1976. Introduction to Ceramics, 2nd ed. Wiley, New York.

Law, R.D., 1990. Crystallographic fabrics: a selective review of their applications to research in structural geology. In: Knipe, R.J., Rutter, E.H. (Eds.), Deformation Mechanisms, Rheology and Tectonics, Special Publications 54. Geological Society, pp. 335–352.

Lister, G.S., Snoke, A.W., 1984. *S–C* Mylonites. Journal of Structural Geology 6, 617–638.

Lloyd, G.E., Freeman, B., 1991. SEM electron channelling analysis of dynamic recrystallisation in a quartz grain. Journal of Structural Geology 13, 945–953.

Means, W.D., 1981. The concept of steady state foliation. Tectonophysics 78, 179–199.

Olesen, N.Ø., Schmidt, N.H., 1990. The SEM/ECP technique applied to twinned quartz crystals. In: Knipe, R.J., Rutter, E.H. (Eds.), Deformation Mechanisms, Rheology and Tectonics, Special Publications 54. Geological Society, pp. 369–373.

Olgaard, D.L., Evans, B., 1988. Grain growth in synthetic marbles with added mica and water. Contributions to Mineralogy and Petrology 100, 246–260.

Panozzo Heilbronner, R., Pauli, C., 1993. Integrated spatial and orientation analysis of quartz *c* axes by computer aided microscopy. Journal of Structural Geology 15, 369–382.

Price, G.P., 1985. Preferred orientations in quartzites. In: Wenk, H.-R. (Ed.), Preferred Orientation in Deformed Metals and Rocks: An Introduction to Modern Texture Analysis. Academic Press, London, pp. 385–405.

Renner, J., Zerbian, A., Stöckhert, B., 1997. Microstructure of synthetic polycrystalline coesite aggregates. The effect of pressure, temperature, and time. Lithos 41, 169–184.

Sander, B., 1950. Einführung in die Gefügekunde der geologischen Körper, Band II: Die Korngefüge. Springer, Wien.

Simpson, C., Schmid, S.M., 1983. An evaluation of criteria to deduce the sense of movement in sheared rocks. Geological Society of America Bulletin 94, 1281–1288.

Smith, C.S., 1964. Some elementary principles of polycrystalline microstructure. Metallurgical Reviews 9, 1–48.

Spry, A., 1969. Metamorphic Textures. Pergamon Press, Oxford.

Stöckhert, B., 1989. Depth and timing of detachment in the Seconda Zona Diorito Kinzigitica, western Alps. Terra abstracts 1, 373.

Stüwe, H.P., 1978. Driving and dragging forces in recrystallization. In: Haessner, F. (Ed.), Recrystallization of Metallic Materials. Riederer, Stuttgart, pp. 11–21.

Tullis, J., Yund, R.A., 1982. Grain growth kinetics of quartz and calcite aggregates. Journal of Geology 90, 301–318.

Twiss, R.J., 1977. Theory and applicability of a recrystallized grain size paleopiezometry. Pure and Applied Geophysics 115, 227–244.

Underwood, E.E., 1970. Quantitative Stereology. Addison-Wesley, Reading, Massachusetts.

Vernon, R.H., 1976. Metamorphic Processes. George Allen & Unwin, London.

Voll, G., 1960. New work on petrofabrics. Liverpool and Manchester. Geological Journal 2, 503–567.

Voll, G., 1961. Zur Frage des Stofftransports auf den Korngrenzen metamorpher Gesteine. Geologische Rundschau 51, 395–405.

Williams, R.E., 1968. Space-filling polyhedron: its relation to aggregates of soap bubbles, plant cells, and metal crystallites. Science 161, 276.